AGU PUBLICATIONS

JGR

Journal of Geophysical Research: Solid Earth

RESEARCH ARTICLE
10.1002/2016JB013864

Key Points:
- New dimensional analysis to scale heating, melting, rounding, and cooling of particles
- Quantitative upper bound on the particle size for thermal equilibrium, melting, and rounding
- Conceptual framework for surface tension-driven dynamics of molten volcanic droplets

Supporting Information:
- Supporting Information S1
- Movie S1

Correspondence to:
F. B. Wadsworth,
fabian.wadsworth@min.uni-muenchen.de

Citation:
Wadsworth, F. B., J. Vasseur, E. W. Llewellin, K. Genareau, C. Cimarelli, and D. B. Dingwell (2017), Size limits for rounding of volcanic ash particles heated by lightning, *J. Geophys. Res. Solid Earth*, *122*, 1977–1989, doi:10.1002/2016JB013864.

Received 15 DEC 2016
Accepted 9 MAR 2017
Accepted article online 10 MAR 2017
Published online 30 MAR 2017

The copyright line for this article was changed on 23 NOV 2017 after original online publication.

Size limits for rounding of volcanic ash particles heated by lightning

Fabian B. Wadsworth[1], Jérémie Vasseur[1], Edward W. Llewellin[2], Kimberly Genareau[3], Corrado Cimarelli[1], and Donald B. Dingwell[1]

[1]Earth and Environmental Science, Ludwig-Maximilians-Universität, Munich, Germany, [2]Department of Earth Sciences, Durham University, Durham, UK, [3]Department of Geological Sciences, University of Alabama, Tuscaloosa, Alabama, USA

Abstract Volcanic ash particles can be remelted by the high temperatures induced in volcanic lightning discharges. The molten particles can round under surface tension then quench to produce glass spheres. Melting and rounding timescales for volcanic materials are strongly dependent on heating duration and peak temperature and are shorter for small particles than for large particles. Therefore, the size distribution of glass spheres recovered from ash deposits potentially record the short duration, high-temperature conditions of volcanic lightning discharges, which are hard to measure directly. We use a 1-D numerical solution to the heat equation to determine the timescales of heating and cooling of volcanic particles during and after rapid heating and compare these with the capillary timescale for rounding an angular particle. We define dimensionless parameters—capillary, Fourier, Stark, Biot, and Peclet numbers—to characterize the competition between heat transfer within the particle, heat transfer at the particle rim, and capillary motion, for particles of different sizes. We apply this framework to the lightning case and constrain a maximum size for ash particles susceptible to surface tension-driven rounding, as a function of lightning temperature and duration, and ash properties. The size limit agrees well with maximum sizes of glass spheres found in volcanic ash that has been subjected to lightning or experimental discharges, demonstrating that the approach that we develop can be used to obtain a first-order estimate of lightning conditions in volcanic plumes.

1. Introduction

Airborne volcanic ash particles that are engulfed by volcanic lightning discharges [*Paxton et al.*, 1986; *Genareau et al.*, 2015], or are ingested by jet engines [*Shinozaki et al.*, 2013; *Song et al.*, 2014, 2016], are subjected to rapid heating. In either case, if a particle's temperature is raised above the glass transition, in the case of glassy ash, or the solidus, in the case of crystalline ash, it behaves as a viscous droplet and becomes susceptible to capillary processes—i.e., deformation induced by the action of surface tension. Capillary processes are important in a variety of phenomena, including droplet rounding and sticking of a droplet to a surface.

Lightning occurs commonly in plumes of volcanic ash produced by moderate to high explosivity eruptions [*McNutt and Williams*, 2010; *Aizawa et al.*, 2016; *Cimarelli et al.*, 2016] and in laboratory experiments of volcanic ash production and proximal transport [*Cimarelli et al.*, 2014]. During discharges, temperatures can reach 10^3–10^4 K [*Paxton et al.*, 1986; *Farzaneh and Chisholm*, 2009; *Rakov*, 2013] and the discharge can take several milliseconds to dissipate [*Paxton et al.*, 1986; *Cimarelli et al.*, 2016]. *Genareau et al.* [2015] suggest that this is sufficient time to heat fine volcanic particles ($<$63 μm diameter) to temperatures well in excess of the glass transition or solidus, and even liquidus, implying that the particles can become fully molten liquid droplets. We propose that this melting allows ash particles, which are initially angular, to round to spherical under the action of surface tension. The observation of abundant glass spheres in deposits of otherwise angular volcanic ash from eruptions such as the 2009 Redoubt eruption (Figure 1) provides tantalizing evidence for this process.

Here we investigate the thermal response of a volcanic particle that is rapidly heated, by applying a nondimensional 1-D spherical heat transfer model. We constrain the critical volcanic particle size below which heat transfer raises the entire particle to a temperature above the glass transition, or a critical melting temperature, in the time available for heat transfer. Then, by way of an example, we focus on the volcanic lightning case. We constrain the timescale for surface tension-driven capillary rounding of the particle, to determine the conditions under which volcanic lighting may transform ash particles into glass spheres.

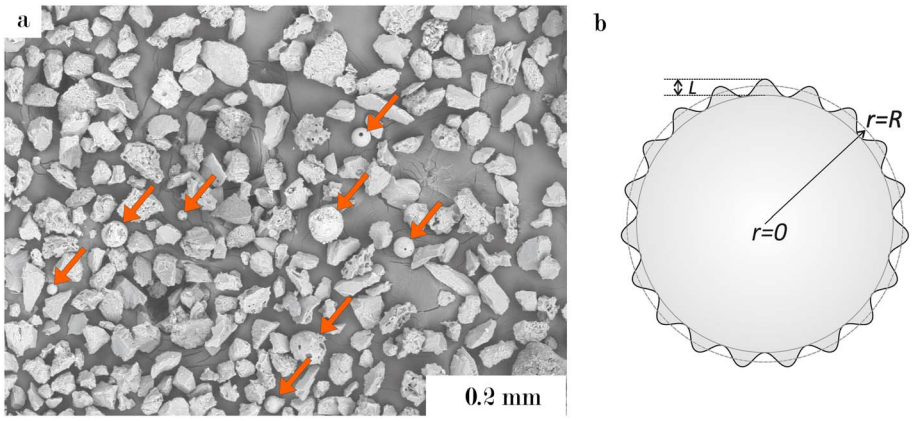

Figure 1. (a) A scanning electron microscopy image of a representative sample from a fall deposit of the 2009 Redoubt eruption for which rounded glass spheres are marked by arrows. (b) The simplified particle geometry used in the model set up where the radial coordinate is r and the asperity length scale is L.

The utility of volcanic lightning as a monitoring tool is being established [*Behnke and McNutt*, 2014], and better constraint of the temperatures, durations, and length scales of volcanic discharges is necessary. Using the framework developed here, minimum temperatures or durations could be extracted from the size distribution of glass spheres found in fall deposits. The framework can also be used to understand the thermal behavior of ash in jet engines, which is crucial to airlines and aviation authorities because molten ash droplets can stick to engine components, causing loss of thrust and engine failure [*Giehl et al.*, 2016]. In what follows we focus primarily on the volcanic lightning case but emphasize that the framework developed in this study is applicable to other scenarios in which thermal disequilibrium is induced at the particle scale.

2. Methods

2.1. Heat Transfer in Spherical Particles

We assess the evolution of the temperature distribution in a spherical particle of radius R using Fourier's law for diffusive heat transfer: $\partial T/\partial t = \nabla(D\nabla T)$, where T is the local temperature, t is time, and D is the thermal diffusivity in the material. Cast in 1-D spherical coordinates [*Crank*, 1975] Fourier's law is

$$r^2 \frac{\partial T}{\partial t} = \frac{\partial}{\partial r}\left(r^2 D \frac{\partial T}{\partial r}\right), \tag{1}$$

where r is the radial distance from the particle center. We explicitly assume that volcanic ash particles are approximately spherical for the heat transfer solution. To justify this, we note that in surveying a large range of glassy volcanic ash particle populations, *Liu et al.* [2015] found that shape factor parameters are close to 1, demonstrating low degrees of asphericity. In Figure 1 the majority of the particles are equant or, where they are irregular in shape, their aspect ratios are close to unity.

The thermal diffusivity of silicate melts and glasses is a function of temperature that can be approximated over a wide range of temperatures, and smoothly across the glass transition interval, by

$$D = D_0 \exp(\alpha T), \tag{2}$$

where D_0 is the extrapolated diffusivity at $T = 0$ (where temperature is in kelvin) and α is a constant. *Bagdassarov and Dingwell* [1994] adopt and parameterize an alternative functional form: $D = 9.14 \times 10^{-7} - 1.4 \times 10^{-9}(T - 273) + 1.9 \times 10^{-12}(T - 273)^2$. The form of $D(T)$ given in equation (2) is more amenable to nondimensionalization (see below). We therefore fit equation (2) to the *Bagdassarov and Dingwell* [1994] expression for $D(T)$ between 823 and 1373 K, which is the range in which the experimental

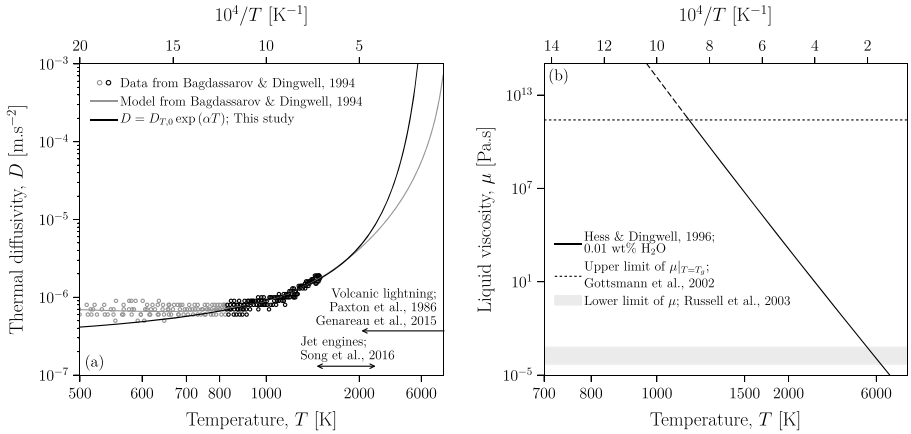

Figure 2. The temperature dependence of physical properties of volcanic ash particles pertinent to this study. (a) The temperature dependence of the thermal diffusivity showing the function provided by *Bagdassarov and Dingwell* [1994] and the fit of equation (2) to this function (fit between 823 and 1373 K using a least squares regression approach). The range of temperatures estimated for high-temperature, rapid heating environments is given for jet engines [*Song et al*., 2016] and volcanic lightning events [*Paxton et al*., 1986; *Genareau et al*., 2015]. (b) The temperature dependence of viscosity for hydrous rhyolitic liquids [*Hess and Dingwell*, 1996] and the coarse definition of T_g used herein [cf. *Gottsmann et al*., 2002].

data show that D is a positive function of T. Below 823 K, *Bagdassarov and Dingwell* [1994] show that D is a negative function of temperature. This dependence is consistent with a phonon-phonon interaction mechanism for heat conduction in solids, while at higher temperatures such as considered in this study, photon conduction is more likely to be the operative mechanism of heat transfer [*Lee and Kingery*, 1960] and D is a positive function of T in this regime. Fitting in this range (823–1373 K), we find that $D_0 = 1.88 \times 10^{-7}\,\mathrm{m^2\,s^{-1}}$ and $\alpha = 1.58 \times 10^{-3}\,\mathrm{K^{-1}}$ with good mutual agreement up to the lower limits of the temperatures typical of volcanic lightning events (>2000 K) [*Genareau et al*., 2015; *Paxton et al*., 1986] and including the operational temperature range of jet engines at cruising altitude (>1300 K) [*Song et al*., 2014, 2016] as well as across all experimental data in this range of temperature (Figure 2). The *Bagdassarov and Dingwell* [1994] relationship is purely empirical and has no validity at the high temperatures that we consider in this study; consequently, we suggest that equation (2) is equally valid. At the temperatures of interest here, the functional form of equation (2) is an approximation of the transition from a thermal diffusivity by phonon interactions at intermediate temperatures to a diffusivity controlled by photon conduction at high temperatures [*Berman*, 1953; *Lee and Kingery*, 1960]. Diffusivity and conductivity are approximately proportional when the temperature dependence of the conductivity is much greater than that of the density or specific heat capacity, which has been shown to be true in natural glasses [*Lange and Carmichael*, 1987; *Bagdassarov and Dingwell*, 1994; *Di Genova et al*., 2014]. We acknowledge that the high-temperature limits to $D(T)$ are potentially unreliable and suggest that they warrant further investigation for silicate materials relevant to geoscience problems.

We consider the case where the spherical particle is heated for a time λ in a gas at homogeneous temperature T'. We assume that the particle is initially in thermal equilibrium at temperature T_i; i.e., $T = T_i$ for all values of r at $t = 0$. At the particle center we assume that the rim is insulated (Neumann boundary condition of 0) such that $D\partial T/\partial r = 0$ for $t > 0$ at $r = 0$. We define the temperature at the particle rim ($r = R$) to be $T = T'$ for $0 < t \leq \lambda$. Following the heating event, the rim temperature decays back to $T = T_i$. In what follows we will first explain the case where the rim of the particle is coupled to the external temperature purely conductively and, subsequently, the more complex case where the particle rim is coupled through a combination of conductive, radiative, and convective heat exchange. For all cases we assume that T_i is an arbitrarily low ambient value of 293 K.

It is useful to define the timescales of the various heat transfer processes, which later form the basis of our nondimensionalization. There are three timescales of relevance, in addition to the timescale of heating λ: λ_{Fo}, which is the characteristic time for conduction to equilibrate temperature differences within the particle; λ_{Bi}, which is the characteristic time for convective heat exchange across the particle surface; and λ_{Sk},

which is the characteristic time for radiative heat exchange across the particle surface. These timescales are given by

$$\lambda_{\mathrm{Fo}} = \frac{R^2}{D};\ \lambda_{\mathrm{Bi}} = \frac{\rho C_p R}{h};\ \lambda_{\mathrm{Sk}} = \frac{\rho C_p R}{\varepsilon \sigma T^3}; \tag{3}$$

where ρ is the material density, C_p is the specific heat capacity, h is a convective heat transfer coefficient, σ is the Stefan-Boltzmann constant ($5.67 \times 10^{-8}\,\mathrm{W\,m^{-2}\,K^{-4}}$), and ε is the emissivity. These quantities are commonly organized into dimensionless groups. The Fourier number $\mathrm{Fo} = t/\lambda_{\mathrm{Fo}} = Dt/R^2$ compares the heating time and the characteristic time for conductive equilibration, such that for small Fo temperature differences induced by the heating event do not have time to equilibrate before the end of the heating. In the simple case where we assume that the particle rim is coupled to the external temperature, $t = \lambda$; however, in the more complex case where convection and radiation limit heat exchange, the time available for heat conduction may be $t < \lambda$. The Biot number $\mathrm{Bi} = \lambda_{\mathrm{Fo}}/\lambda_{\mathrm{Bi}} = hR/\rho C_p D$ compares the characteristic times for conductive equilibration and for convective heat transfer across the particle surface, such that for small Bi thermal equilibration following a temperature change is limited by convection at the surface, rather than conduction within the particle. The Stark number $\mathrm{Sk} = \lambda_{\mathrm{Fo}}/\lambda_{\mathrm{Sk}} = \varepsilon\sigma T^3 R/\rho C_p D$ compares the characteristic times for conductive equilibration and for radiative heat transfer across the particle surface, such that for small Sk thermal equilibration following a temperature change is limited by radiation at the surface, rather than conduction within the particle. We also define two further dimensionless groups:

$$\mathrm{FoBi} = \frac{t}{\lambda_{\mathrm{Bi}}} = \frac{ht}{\rho C_p R};\ \mathrm{FoSk} = \frac{t}{\lambda_{\mathrm{Sk}}} = \frac{\varepsilon\sigma T^3 t}{\rho C_p R}, \tag{4}$$

These compare the heating time and, respectively, the characteristic times for convective and radiative heat transfer across the particle surface. For small FoBi and small FoSk, transfer of heat across the surface of the particle on the timescale of the heating event is limited, respectively, by convective and radiative processes.

For conduction inside the particle, we nondimensionalize the heat transfer problem by making the following substitutions:

$$\overline{T} = \frac{T}{T'};\ \overline{r} = \frac{r}{R};\ \overline{t} = \frac{t}{\lambda};\ \overline{D} = \frac{D}{D'};\ \mathrm{Fo}' = \frac{D'}{R^2}\lambda;\ \overline{\alpha} = \alpha T', \tag{5}$$

where we use a bar above a parameter to denote that it is in dimensionless form. Here D' is the thermal diffusivity at T' such that $D' = D_0 \exp(\alpha T')$, and Fo′ is the Fourier number assessed at T'. Now equations (1) and (2) can be expressed in dimensionless form, respectively,

$$\frac{\partial \overline{T}}{\partial \overline{t}} = \mathrm{Fo}' \left[\frac{\partial}{\partial \overline{r}} \left(\overline{D} \frac{\partial \overline{T}}{\partial \overline{r}} \right) + \frac{2}{\overline{r}} \left(\overline{D} \frac{\partial \overline{T}}{\partial \overline{r}} \right) \right], \tag{6}$$

$$\overline{D} = \exp\left[\overline{\alpha} \left(\overline{T} - 1 \right) \right], \tag{7}$$

The boundary condition at the particle center becomes, in dimensionless form, $\overline{D}\partial\overline{T}/\partial\overline{r} = 0$ for $\overline{t} > 0$ at $\overline{r} = 0$. For the first and simpler case where the particle is conductively coupled to the temperature outside the particle, the boundary condition at the particle rim is $\overline{T} = 1$ at $\overline{r} = 1$ for $0 < \overline{t} \leq 1$ and $\overline{T} = T_i/T'$ at $\overline{t} > 1$. For the more complex case where the particle rim exchanges heat with the surrounding gas through a combination of conduction, radiation, and gas convection, we must consider the heat flux through the particle rim. Given that we are interested in relatively high imposed T', the appropriate thermal boundary condition for $r = R$ is the sum of a radiative and convective flux such that

$$D\frac{\partial T}{\partial r} = \underbrace{\frac{\sigma\varepsilon}{\rho C_p}}_{\text{radiative}} T^4 + \underbrace{\frac{h}{\rho C_p}}_{\text{convective}} T \text{ for } t > 0 \text{ at } r = R. \tag{8}$$

Throughout, we take ρ, C_p, and h to be negligibly dependent on temperature and use constant values of $\rho = 2000\,\mathrm{kg\,m^{-3}}$ [*Lange and Carmichael*, 1987], $C_p = 1000\,\mathrm{J\,kg^{-1}\,K^{-1}}$ [*Di Genova et al.*, 2014], and $h = 100\,\mathrm{W\,m^{-2}\,K^{-1}}$ [*Stroberg et al.*, 2010]; these values are typical of anhydrous silicate liquids. Of these

parameters, h is the least well constrained in our work because its value depends on whether the convection at the particle rim is forced or natural, which in turn depends on wind conditions or particle velocities relative to the plume gas [*Stroberg et al*., 2010]. We use the value selected as a median between end-member possibilities for volcanic particles, and in the supporting information we show how the main results of this manuscript are altered by changing h by orders of magnitude ($10 \le h \le 1000\ \mathrm{W\,m^{-2}\,K^{-1}}$). Equation (8) is rendered nondimensional as follows:

$$\overline{D}\frac{\partial \overline{T}}{\partial \overline{r}} = \mathrm{Sk}'\,\overline{T}^4 + \mathrm{Bi}'\,\overline{T} \text{ for } \overline{t} > 0 \text{ at } \overline{r} = 1, \tag{9}$$

where Sk′ and Bi′ are the Stark and Biot numbers assessed at T' (hence, diffusivity in those terms is D').

We solve equation (6) numerically using a fully implicit finite-difference scheme (i.e., backward time, centered-space) coupled with a relaxed fixed-point method to ensure convergence at each time step. We employ a dimensionless spatial resolution of 10^{-2} and a dimensionless temporal resolution of 10^{-4}.

2.2. Rounding of Volcanic Ash Particles

In order to change shape, the particle must be sufficiently hot to behave as a viscous liquid. To define the conditions under which the material can be considered a viscous liquid, we treat the particles as if they are made entirely of volcanic glass with a homogeneous composition; hence, we do not consider the kinetics of melting a crystalline or a partially crystalline particle. This is justified as the composition of volcanic ash and of the experimental particles used in flashover experiments compiled in *Wardman et al*. [2012] is typically dominated by volcanic glass [*Heiken*, 1974]. Consequently, the temperature of the glass transition represents the thermal limit above which the liquid can relax and respond viscously. The transition of a glass to a liquid has been investigated experimentally using natural silicates [*Dingwell and Webb*, 1989] in thermal disequilibrium scenarios. Although still enigmatic in detail, the temperature position of the glass transition is empirically related to the temperature dependence of liquid viscosity μ [*Angell et al*., 2000]. This temperature dependence can be well parameterized by a Vogel-Fulcher-Tammann (VFT) equation of the form $\log_{10}(\mu) = A + B/(T - C)$. We follow the model proposed by *Hess and Dingwell* [1996] in which A, B, and C, are related to the dissolved water content and have been calibrated for calc-alkaline rhyolitic liquids. For 0.01 wt % water considered here (see below), $A = -7.38$, $B = 20{,}506.04$, and $C = 47.18$. The glass transition temperature is apparently dependent on the temperature rate at which it is crossed [*Gottsmann et al*., 2002]. Over a measured range of cooling rates of 1–20 $\mathrm{K\,s^{-1}}$, *Gottsmann et al*. [2002] found that the viscosity of natural glasses at the glass transition ranges from ~10^9 to ~10^{12} Pa s. However, it remains unclear how the glass transition relates to heating or cooling rate in materials for which there is a strong spatial distribution of temperature, such as considered here [*Pijpers et al*., 2002]. Therefore, for simplicity, we define the glass transition in terms of a threshold viscosity, taken as $10^{11.4}$ Pa s [*Gottsmann et al*., 2002]; above this viscosity the material is a glass, and below this viscosity the material is a viscous liquid. Assuming 0.01 wt % dissolved water concentration, which is a typical value for rhyolites erupted into the atmosphere or for rhyolites that have been reheated to the high temperatures considered herein [*Liu et al*., 2005], we use the VFT parameterization to determine T_g as the temperature at which $\mu = 10^{11.4}$ Pa s. This provides a starting criterion on heating at which we consider the particle to be a viscous liquid, rather than a solid glass (Figure 2). We consider a temperature range outside the measured calibration of the *Hess and Dingwell* [1996] viscosity model, and as such, we also show that the highest temperatures considered here (6000 K) are also consistent with the theoretical lower limit to μ for silicate liquids [*Russell et al*., 2003].

As soon as the outermost part of the ash particle has melted, surface tension can begin to act to relax its irregular surface toward spherical. In general, we expect that surface irregularities of a given length scale L (see Figure 1b) can be relaxed only once the melting front has reached to a similar depth within the particle; consequently, to round the particle completely requires that the melting front reaches to the center of the particle. In order to relax this assumption, a much more sophisticated treatment would be required, which explicitly considers the initial shape of the particle and the capillary flow within the growing molten film during heating. Such an approach would presumably find that particles that deviate only slightly from spherical would be able to round without melting to the center, in the case where capillary rounding is fast compared with heating. The characteristic timescale for heat to penetrate to the center of a volcanic particle

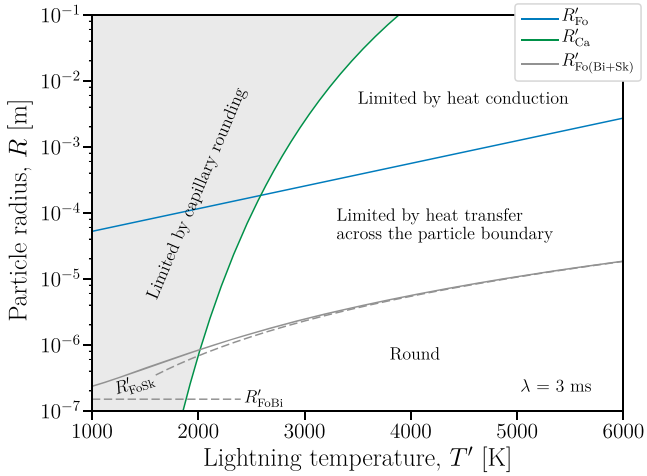

Figure 3. The radius limits to the capillary and heat transfer processes considered (see text) when no gradients of temperature exist on the particle scale and where the timescale available for each process is the lightning duration λ (plotted here is an example for $\lambda = 3$ ms).

during the lightning discharge is the Fourier timescale λ_{Fo} (equation (3)). The time required to reach a temperature at which $\mu \leq 10^{11.4}$ Pa s everywhere in the particle, which we term λ_c, is not always equal to λ_{Fo} (see section 3).

The timescale for viscous relaxation is approximated by the capillary time λ_{Ca}, which is the characteristic time for rounding isolated droplets by the action of surface tension. The capillary time is given by

$$\lambda_{Ca} = \frac{R\mu}{\Gamma}, \tag{10}$$

[e.g., *Rallison*, 1984], where Γ is the melt-vapor interfacial tension. The same definition has been used as a characteristic timescale in the sintering of spherical viscous droplets [*Wadsworth et al.*, 2014, 2016] because sintering also involves the relaxation of melt droplet surfaces and in studies of bubbles relaxing in a viscous liquid [*Taylor*, 1934; *Llewellin et al.*, 2002]. In all cases the stress driving the relaxation of the fluid droplet to a sphere arises from Γ which confers an excess surface pressure $P \propto \Gamma/R$.

The time required for capillary processes, λ_{Ca}, can be compared with the time t that is available for rounding, yielding another dimensionless group, the capillary number $\mathrm{Ca} = \lambda_{Ca}/t = R\mu/\Gamma t$. If heating and cooling of the particle were instantaneous, then we would have $t = \lambda$; however, heating and cooling are limited by conduction, convection, and radiation, as discussed in the previous section. In general, therefore, $t > \lambda$. Recalling the dimensionless heat transport numbers defined in the previous section, we now have a set of dimensionless groups that describe surface tension-driven rounding (Ca), conduction within the particle (Fo), and heat exchange across the particle rim via convection (FoBi) and radiation (FoSk). We adopt the simple assumption that unity divides regimes of behavior in this set of dimensionless groups, allowing us to set each group equal to unity and rearrange to find the particle radius above which rounding is limited by the process in question. In the case of the capillary number, $R_{Ca} = \Gamma t/\mu$ is the particle radius above which we would not expect rounding to complete. In the case of the Fourier number, $R_{Fo} = \sqrt{Dt}$ is the radius above which we would not expect conductive thermal equilibration inside the particle. In the case of FoBi and FoSk, $R_{Bi} = ht/\rho C_p$ and $R_{Sk} = \varepsilon\sigma T^3/\rho C_p t$ are the radii above which we would not expect the rim temperature to have equilibrated with the external temperature by convective or radiative heat transfer, respectively. Finally, the critical time beyond which all of the particle interior is heated above T_g, which is λ_c, relates to a critical radius limit R_c.

In all cases we consider $\mathrm{Ca} < 1$ to be the primary criterion for rounding to occur (equivalently, $R < R_{Ca}$). The time available for rounding depends on thermal processes, and we propose that $R < R_{Fo}$, $R < R_{Bi}$, and $R < R_{Sk}$ represent criteria for the different heat transfer processes to complete.

In Figure 3, we explore these limiting radii as functions of lightning temperature and duration. For this analysis, we assume isothermal conditions at lightning temperature for all parameters ($T = T'$; $D = D'$; $\mu = \mu'$) and we adopt $t = \lambda$ for the capillary number and Fourier number. Under these assumptions, the limiting radii become R'_{Ca}, R'_{Fo}, R'_{Sk}, and R'_{Bi}. We additionally show the radius $R'_{Fo(Bi+Sk)'}$ which accounts for both convective and radiative processes at the particle surface and has the desirable limits of R'_{Bi} and R'_{Sk} at low and high T', respectively.

In reality, during rapid heat transfer in a lightning discharge, gradients of temperature exist on the particle length scale, and these gradients evolve with time; hence, the value of temperature-dependent quantities (D and μ) varies radially. Furthermore, the time available for rounding may be limited by heat conduction,

and the time available for heat conduction may be limited by the transfer of heat at the particle surface; consequently, $t = \lambda$ may not be the relevant timescale for the capillary and Fourier numbers, and the conditions $\mathrm{Ca} < 1$ and $\mathrm{Fo} > 1$ may be met during heating at $t \leq \lambda$ or during cooling at $t > \lambda$. The regime limits may, therefore, be more complex than the isothermal example presented in Figure 3. We can calculate the evolution of the temperature gradients explicitly via equations 4–7, so we can integrate the temperature-dependent parameters over the particle radius, yielding an average value of these dimensionless groups. Here we use angular brackets around a parameter, e.g., $\langle \cdot \rangle$, to indicate that it contains an integrated average of the spatial distribution of the values of temperature-dependent quantities, such that

$$\langle \cdot \rangle = \int_0^1 (\cdot) \mathrm{d}\bar{r} \,, \tag{11}$$

where $(\cdot)$ represents any of the dimensionless parameters. The dimensionless groups Ca and Fo then become

$$\langle \mathrm{Ca} \rangle = \frac{R}{\Gamma' t} \int_0^1 \mu \, \mathrm{d}\bar{r}; \langle \mathrm{Fo} \rangle = \frac{t}{R^2} \int_0^1 D \, \mathrm{d}\bar{r} \,. \tag{12}$$

As FoBi is temperature independent and FoSk is simply related to the cube of temperature, and because neither dimensionless group contains additional temperature-dependent parameters, they do not require integration. That implies that FoSk and FoBi are independent of internal gradients of temperature inside the particles.

To find R_{Ca} and R_{Fo}, we must then assess the evolution of $\langle \mathrm{Ca} \rangle$ and $\langle \mathrm{Fo} \rangle$ with t and find the maximum radius above which the condition $\langle \mathrm{Ca} \rangle \leq 1$ or $\langle \mathrm{Fo} \rangle \geq 1$ is not met in the time available. The definition of the available time is simply λ in the case of pure conduction (section 3.1). In the more complex case where the rim temperature is limited by convection and radiation during and after the lightning, then the time available can be extended beyond λ until the rim of the particle cools below T_g, after which rounding is impossible (section 3.2).

3. Numerical Results and Regimes of Behavior

3.1. The Pure Conduction Case

In this section we apply the general theoretical constraints outlined above to the problem of volcanic ash particles heated in lightning discharge events where the heating is purely conductive. In Figure 4 we show the calculated temperature distribution in particles with different radii at the end of a heating event that lasts 3 ms (i.e., $\lambda = 3$ ms) at $T' = 3273$ K, which represents conditions consistent with volcanic lightning discharges that are a few meters in length [*Cimarelli et al.*, 2016]. In this example only the heating portion ($t \leq \lambda$) is considered, because the particle surface is assumed to drop to $T = T_i < T_g$ at $t > \lambda$, after which no further rounding is possible. The subsequent cooling is discussed later, in section 3.2.

In Figure 4 we explicitly compute R_c and R_{Fo} (using equation (12) to find the value of R for which $\langle \mathrm{Fo} \rangle = 1$ at $t = \lambda$) and show that they are in approximate agreement for a range of T' and that $R_c \rightarrow R_{\mathrm{Fo}}$ at high T' (Figure 4 inset). This means that we can approximate R_c as R_{Fo} under this heating scenario; hence, the conditions for a particle to round are that $T' > T_g$ and that both $\langle \mathrm{Fo} \rangle \geq 1$ and $\langle \mathrm{Ca} \rangle \leq 1$; equivalently, that both $R \leq R_{\mathrm{Fo}}$ and $R \leq R_{\mathrm{Ca}}$.

When all conditions for rounding are met, the rounding may be limited either by the rate of thermal diffusion or by the rate of capillary processes. For the pure conduction case, we can additionally determine which process is limiting by comparing $\langle \mathrm{Fo} \rangle$ and $\langle \mathrm{Ca} \rangle$ to find a capillary Peclet number $\langle \mathrm{Pc} \rangle$. In thermal equilibrium $\mathrm{Pc} = \mathrm{CaFo} = \mu D / \Gamma' R$ or, in the case of thermal disequilibrium, $\langle \mathrm{Pc} \rangle = \int_0^1 \mu D \mathrm{d}\bar{r} / \Gamma' R$. If $\langle \mathrm{Pc} \rangle \ll 1$, capillary rounding is fast compared with heat diffusion; consequently, the shape evolution of the particle reflects the shape of the advancing T_g isotherm. In this case, the particle is round as soon as T_g is reached in the center. If $\langle \mathrm{Pc} \rangle \gg 1$, heat diffuses quickly compared with capillary rounding, such that the whole particle may be molten whilst it still has an irregular shape. As with the Fourier and capillary numbers, we can rearrange to find the radius at which $\langle \mathrm{Pc} \rangle = 1$, which we term R_{Pc}.

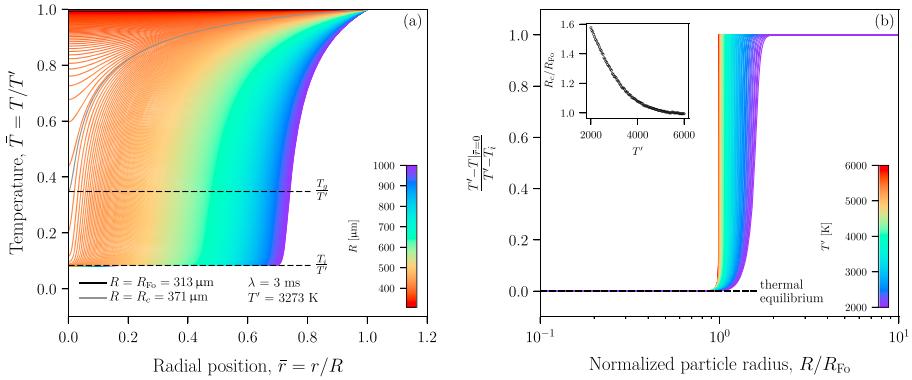

Figure 4. The distribution of temperature in particles of a range of sizes at the end of a heating event of 3 ms duration. Heat transfer across the rim of the particle (at $\bar{r} = 1$) is neglected: the rim is instantaneously heated to T' at $t > 0$ and cools instantaneously to T_i at $t = \lambda$. (a) Example temperature profiles within ash particles for $T' = 3273$ K and $\lambda = 3$ ms; a range of particle radii ($R \leq 1$ mm) is considered given in the color scale bar. The profile for a particle with R_c, for which the temperature at the particle center just meets T_g at $t = \lambda$, is shown as a grey curve; for these conditions, $R_c = 371$ μm. The profile for a particle with $R_{Fo} = 313$ μm is also displayed but is imperceptible near the $\bar{T} = 1$ limit (equilibrium). (b) A measure of the difference in temperature between the particle center and particle rim assessed at λ for a range of R and T' (independent of λ), showing that R_{Fo} approximates the equilibrium limit. We note that $R_c \rightarrow R_{Fo}$ in the high-temperature limit (inset).

For anhydrous rhyolitic silicate melts, typical of the most explosive volcanic eruptions, which are those likely to produce lightning [*McNutt and Williams*, 2010], $\Gamma \approx 0.3$ N m^{-1} and is approximately temperature independent [*Gardner and Ketcham*, 2011]. We note that as yet, no experimental data are available at the high temperatures considered here. If we take the case example of a volcanic lightning discharge with $T' = 3273$ K and $\lambda = 3$ ms, and a dissolved water concentration in the volcanic ash of 0.01 wt %, we find that $R_{Fo} = 0.31$ mm (which agrees well with $R_c = 0.37$ mm; Figure 4) and $R_{Ca} \approx R_c$. In this case, therefore, Fourier number is limiting and ash particles smaller than R_{Fo} would be expected to be rounded, whilst larger particles would remain angular. At R_{Fo}, the value of Pc is 0.035 (below unity), which confirms that the Fourier number is limiting in this case (Figure 5a).

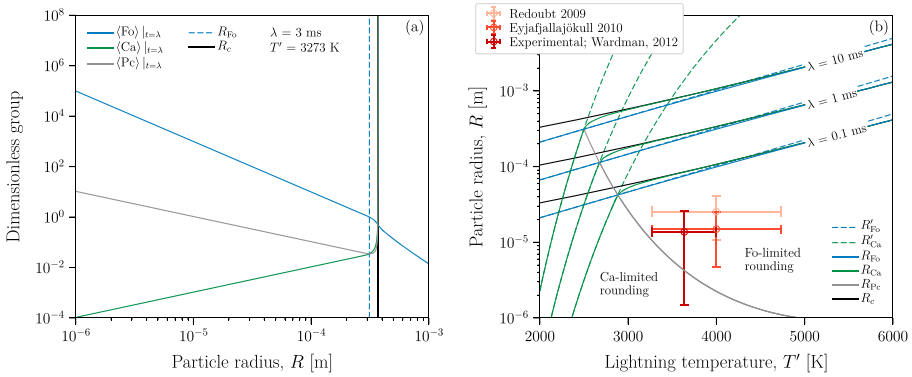

Figure 5. Results for the simple case when particles are heated by conduction alone. (a) The dependence of the dimensionless groups ⟨Ca⟩, ⟨Fo⟩, and ⟨Pc⟩ on particle radius, assessed at the end of a lightning discharge of temperature $T' = 3273$ K and duration $\lambda = 3$ ms. For $R < R_{Fo}$, the isothermal conditions of the lightning approximate the parameters as the particles are in thermal equilibrium. (b) The dependence of the critical particle radii R_{Ca}, R_{Fo}, and R_c on T'; R_{Pc} is also shown, which is the radius at which Pc = 1; i.e., the radius that divides the regimes in which Ca and Fo are limiting (labeled). Ash particles that fall below and to the right of both the green and blue curves will round by the end of the heating event. Glass spheres formed in experimental discharges with temperature $3273 < T' < 4000$ K [*Farzaneh and Chisholm*, 2009; *Wardman et al.*, 2012] have radii $1.5 < R < 26$ μm, and glass spheres found in natural deposits from explosive eruptions have radii $10.6 < R < 40.4$ μm (Redoubt 2009) and $4.75 < R < 25.15$ μm (Eyjafjallajökull 2010). These data fall in the "round" region of this plot, and R_{Pc} shows that the rounding of these particles was limited by Fo and not Ca. For the 2010 Eyjafjallajökull and 2009 Redoubt eruptions we estimate $3000 < T' < 5000$ K on the basis of lightning discharge models and observations [*Paxton et al.*, 1986; *Farzaneh and Chisholm*, 2009], but we note that T' could be higher.

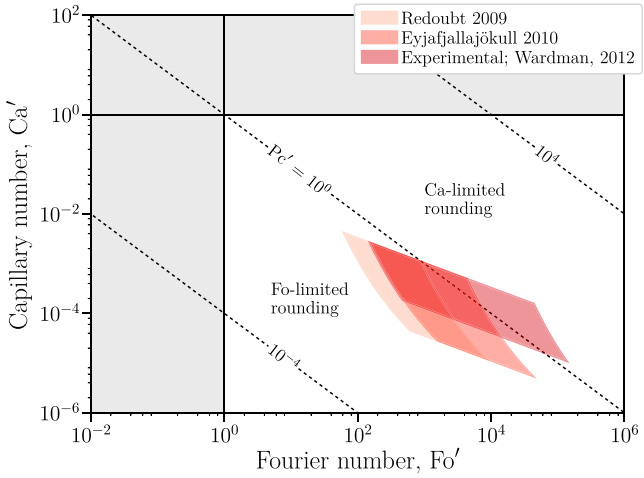

Figure 6. An isothermal approximation of the rounding analysis for which Fo and Ca are assessed at the isothermal conditions of the lightning discharge (termed Fo′ and Ca′); the position of the naturally and experimentally observed glass spheres is plotted assuming $\lambda = 3$ ms and using the range of measured radii. This simple analysis is especially accurate if conduction can be assumed to be the dominant heat transfer process and if $R < R_{Fo}$ (see Figure 5). Above Ca′ = 1 and below Fo′ = 1, rounding is impossible (grey shaded area). The fields where Ca or Fo are limiting are labeled, respectively.

In Figure 5a we show how ⟨Ca⟩, ⟨Fo⟩, and ⟨Pc⟩, assessed at $t = \lambda$, depend on the particle radius. For $R < R_{Fo}$, the curves are linear in R, indicating that the isothermal forms of Ca′ and Fo′ (from equation (3)) and Pc' are sufficient. For $R > R_{Fo}$, the curves have a nonlinear dependence on R and the nonisothermal forms ⟨Ca⟩ and ⟨Fo⟩ (equation (12)) and ⟨Pc⟩ must be used. In Figure 5b we show how R_{Ca}, R_{Fo}, R_c, and R_{Pc}, assessed at $t = \lambda$, depend on the temperature T'. Our predicted values of the maximum radius of rounded particles exceed the upper limits of the glass spheres found in deposits resulting from electrical flashover experiments (~1.5–26 μm) [*Wardman et al.*, 2012] and found in natural volcanic fall deposits [*Genareau et al.*, 2015] such as from the 2010 eruption of Eyjafjallajökull volcano and the 2009 eruption of Redoubt volcano (Figure 1; ~5–40 μm) confirming that these particles can indeed be rounded in heating events with $\lambda \geq 0.1$ ms. Furthermore, the analysis indicates that rounding of the natural and experimental particles was limited by thermal diffusion, rather than capillary rounding (i.e., rounding is Fo limited; Figure 5b).

Figure 5b shows that the rounding condition ⟨Ca⟩ = 1, given by R_{Ca}, approaches asymptotic limits at high and low T'. At low T', R_{Ca} collapses to the isothermal R'_{Ca}, showing that at low temperatures, the rounding is controlled by viscosity rather than heat transfer. At high T', R_{Ca} approaches both R_c and R_{Fo} and is also similar to the isothermal R_{Fo}, showing that at high temperatures, rounding is controlled by thermal diffusion. Therefore, to a first order, in the conduction-only case, the isothermal R'_{Ca} limits low-temperature rounding and the isothermal R'_{Fo} limits the high-temperature rounding.

For this conduction-only case, the isothermal values of Ca′ and Fo′, and the associated radii R'_{Ca} and R'_{Fo}, are sufficient to provide an approximate description of the rounding behavior. These isothermal quantities have the practical advantage that they can be evaluated trivially and do not require a numerical solution. In Figure 6 we plot the position of the natural and experimental glass spheres in Ca′-Fo′ space, assuming a typical lightning duration of $\lambda = 3$ ms.

3.2. The Case of Conduction, Convection, and Radiation

Surface tension-driven rounding requires that the rim of the particle is liquid (i.e., $T > T_g$ at $r = R$). In the conduction-only case discussed in the previous section, this condition is met immediately upon commencement of the heating event (as long as $T' > T_g$). Similarly, in that scenario, the temperature at the rim falls immediately below T_g when the lightning ceases. However, when radiative and convective heat transfer across the particle rim (equations (4), (8), and (9)) is considered during heating and cooling (during and after the lightning discharge), the condition where the rim is above T_g is only reached after a finite time on heating and must persist for finite time once the heating ceases and the particle is returned to a relatively cool environment at T_i. Here we extend our analysis to consider the time available for rounding when heat gain and loss are kinetically limited by radiation of heat to and from the particle and convection in the surrounding air at the rim. In this more complex case, it is no longer useful to assess the dimensionless groups at $t = \lambda$ Rather, we first find the size limit on particles that are brought completely above T_g at some point during the heating and cooling cycle such that $R \leq R_c$ and, for that class of particles, we find the radius limits below which Fo ≥ 1 and Ca ≤ 1 at some point before the rim of the particle cooled again to T_g.

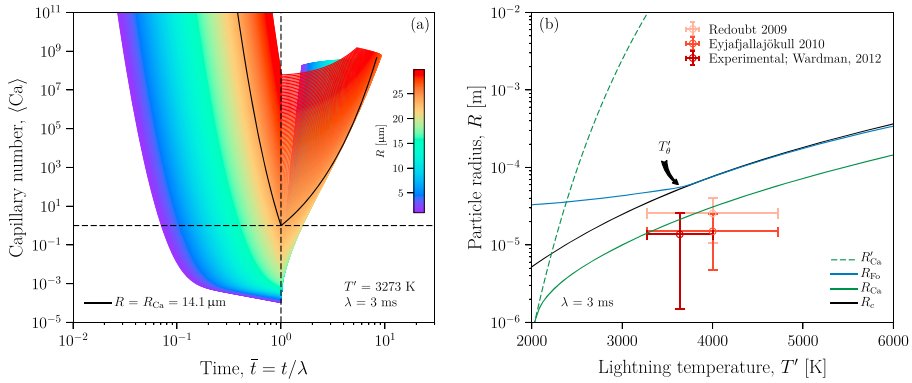

Figure 7. Extension of the scaling considered in Figure 4 for the case when radiative and convective cooling at the particle rim is considered during and after the heating event. (a) An example for $T' = 3273$ K and $\lambda = 3$ ms where we show how $\langle Ca \rangle$ can evolve with time toward minima at $t = \lambda$. In this case $R_{Ca} \approx 18$ μm (compare with $R_{Ca} \approx 371$ μm in Figure 5). (b) The limits on the critical radii for rounding volcanic ash particles.

In our analysis we take ρ, C_p, and h to be independent of temperature (values are given following equation (8)). We find that the length of time for which the particle rim is maintained above T_g on cooling does not depend strongly on the emissivity ε; therefore, for this scaling analysis, we consider the particles to be perfect black bodies (i.e., $\varepsilon = 1$). In Figure 7a we show that if $Ca \leq 1$ was not met on heating, it cannot be met on cooling either, rendering the cooling step irrelevant for constraint of R_{Ca}. However, R_{Ca} is still quite different from the case where convection and radiation were neglected on heating (Figure 5). This is because the thermal lag at the rim on heating retards the temperature increase in the particle with respect to the lightning temperature T' even if the conduction in the particle is highly efficient. The radii limits presented in Figure 5b can be refined to include these additional constraints (Figure 7b). Those radii limits are all decreased to lower values when thermal exchange at the rim is included, pushing the scaled window for rounding of volcanic ash particles toward the range of measured radii from natural and experimental deposits. A lightning duration of $\lambda = 3$ ms would produce R_{Ca} that are most consistent with the upper limits of the radii measured. This time is consistent with recent observations of lightning discharge durations at Sakurajima volcano, which average $\lambda = 2.5$ ms [*Cimarelli et al.*, 2016].

We can additionally find the radius below which $T < T_g$ for all r and at all times, which represents the particle size limit above which the particle remained entirely solid throughout the heating and cooling and which therefore did not change shape at all. As before, this radius limit is R_c and we include it in Figure 7b, for a lightning duration of $\lambda = 3$ ms. We note that the range of radii measured for rounded particles falls entirely below this limit.

In this scenario, Fo represents the measure of equilibrium between the average particle temperature and the temperature at the particle rim, which is controlled by FoSk and FoBi. At low T', R_{Fo} approaches the temperature-independent slope, typical of R_{FoBi}, and at high T', R_{Fo} approaches the slope of the temperature dependence of R_{FoSk} (compare with Figure 3). This is not surprising as at low T', radiation is negligible and so conduction and convection dominate, whereas at high T', radiation dominates. The inflection in R_{Fo} occurs at a temperature T'_θ which also represents the temperature above which R_{Fo} is met on cooling and below which R_{Fo} is met on heating (Figure 7). As with the conduction-only case, at low T', the isothermal R'_{Ca} is a sufficient description of the rounding condition R_{Ca}. And at the high T' limit, R_{Ca} approaches R_{Fo} and R_c. Unlike the conduction-only case, this high-temperature limit has no isothermal equivalent because the isothermal R'_{Fo} is complicated by the effect of the radiative and convective rim conditions.

4. Discussion

The temperature of lightning discharges has been constrained for lightning events, in general, by numerical models [*Paxton et al.*, 1986], and the duration of volcanic lightning discharges has been constrained by direct observation [*Cimarelli et al.*, 2016]. The scaling analysis presented above provides an alternative framework that could be used to estimate the temperature or duration of lightning discharge events from the size

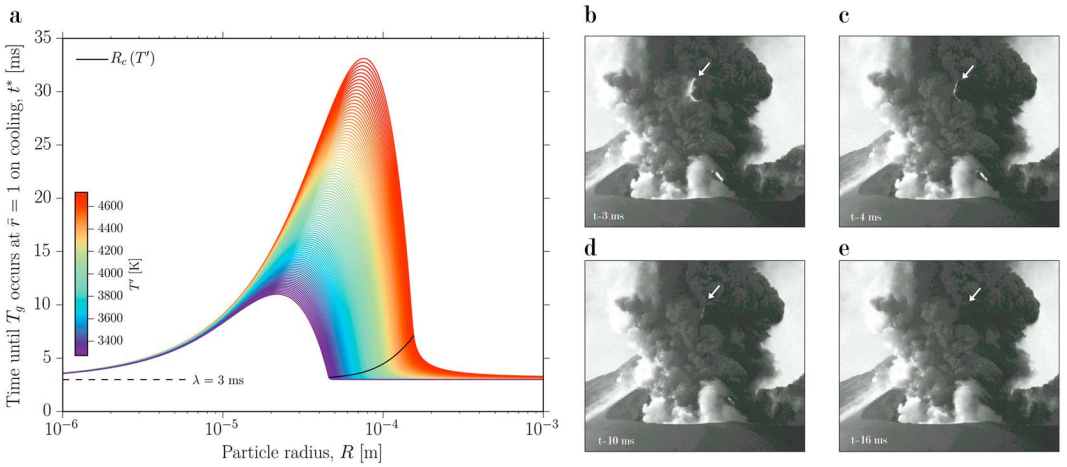

Figure 8. (a) The dependence on the time required for the particle rim to cool to T_g after $t = \lambda$ on T' and R. Shown for reference is the R_c for each value of T', and we note that particles larger than these values did not fully melt on heating. (b–e) Observations from the 27 October 2013 eruption of Sakurajima volcano filmed at 3000 frames per second demonstrating that after a peak discharge intensity (Figure 8b), the discharge afterglow is sustained for time t^* (in this case $t^* = 16$ ms). Times recorded from the first indication of discharge are $t = \lambda = 3$ ms (Figure 8b), 4 ms (Figure 8c), 10 ms (Figure 8d), and $t = t^* = 16$ ms (Figure 8e).

ranges of rounded ash particles. If T' and λ are constrained, the range of likely discharge currents could in turn be estimated, if coupled with a return stroke model [*Paxton et al*., 1986]. This would be valuable to the current effort to render lightning monitoring as a useful tool for constraining volcanic plume conditions, such as overpressure at the vent, particle size distributions [*Cimarelli et al*., 2014], and mass discharge rates. We note that while the peak temperatures of lightning discharges in large thunderstorms are much higher than in volcanic discharges [*Paxton et al*., 1986], the particle fraction of suspended atmospheric dust is much lower than that of volcanic ash in a plume. This may explain why glass spheres resulting from nonvolcanic lightning events have not been reported, despite conditions for rounding of droplets being favorable (high T' and λ).

To explore another example of how direct observations of lightning events at active volcanoes could be used to extract information about plume conditions, we show an example in which particle size information may be recorded in discharge dynamics. First, we use the full model here presented to show that there is a strong dependence of the time required for the particle rim ($\bar{r} = 1$) to fall to T_g on cooling ($t > \lambda$ on T' and R for $\lambda = 3$ ms (Figure 8). This cooling timescale t^* may correlate with the time of the postdischarge afterglow witnessed in real events [*Aizawa et al*., 2016]. The afterglow time is estimated to extend after λ for 0.166–26 ms (videography constraints presented in *Aizawa et al*. [2016]). In Figure 8 we show still images from one such video taken at Sakurajima volcano in Japan (from an eruption on 27 October 2013; video in the supporting information) that represent the peak discharge intensity (Figure 8b) and two times after the peak. We interpret a significant component of this afterglow time in an intraplume discharge event to arise from the relatively slow cooling of the rapidly heated ash particles. This would suggest that a maximum afterglow time would relate to maximum cooling particle sizes of ~150 μm and the peak lightning temperature would be more consistent with the upper limits considered herein (≥4400 K) than the lower values (Figure 8). This analysis of afterglow timescales coupled with the heat transfer model potentially provides a direct way in which volcanic lightning observations can be used as a monitoring tool for constraining particle size distributions or maxima in plumes. In principle, a polydisperse solution to the scaling arguments used here for R_{Ca} could be applied if a distribution type for proximal volcanic ash particle sizes were known.

The scaling analysis presented is generally applicable to scenarios in which small silicate particles are melted and undergo processes associated with surface tension-driven viscous flow. We focus on the lightning case as an applied example of our scaling. Although not treated in detail, the analysis is applicable to other situations in which volcanic ash is rapidly heated to temperatures in excess of the glass transition or solidus temperature and becomes subject to capillary forces; these conditions are met in combustion chambers of jet engines during operation [*Shinozaki et al*., 2013; *Song et al*., 2016]. The analysis of the conditions under which volcanic

ash will strike and adhere to a jet engine surface is more complex than the thermal and capillary analysis presented here and involves additional scaling parameters [*Shinozaki et al.*, 2013]. However, whether a particle will stick and deposit on surfaces or not is known to be related to Ca when the Weber number at impact is low [*Schiaffino and Sonin*, 1997], where the Weber number, $We = \rho u^2 R/\Gamma$, scales the importance of the particle inertia arising from its flight velocity u. Particles ingested in jet engines are typically $R < 30$ μm [*Kueppers et al.*, 2014], temperatures are of the order of $T' = 1340$–2600 K [*Shinozaki et al.*, 2013; *Song et al.*, 2016], and flight duration in the combustor is $\lambda = 1$ ms [*Shinozaki et al.*, 2013]; hence, our analysis shows that these particles are likely to be completely molten and in thermal equilibrium at $t = \lambda$, because $Fo \gg 1$ (Figure 3). This potentially simplifies the scaling appropriate for assessing the dynamics of the impact of molten volcanic droplets on jet engine surfaces.

5. Concluding Remarks

In this study we have shown that the rounding of volcanic ash particles can be limited by the rate of thermal diffusion within the particle, the rate of thermal exchange across the particle surface, or by the rate of capillary flow, and we have explored the conditions that dictate the relevant regime. In doing so we have found fundamental upper bounds on the radii of particles that can be expected to round when subjected to a heating event of given temperature and duration. We analyze example scenarios in which ash is heated by natural or experimental lightning discharges, showing that the size of the rounded particles is consistent with our model and that the round particles formed in the diffusion-limited regime. Future work could apply this theoretical framework to (1) extend the utility of lightning monitoring at active volcanoes by using round particles in deposits to constrain temperatures and durations of discharges, (2) extend our analysis to investigate the conditions under which ash particles can melt and stick to surfaces in jet engine turbines, and (3) couple the scaling arguments we present with other capillary-driven processes of volcanic relevance, such as relaxation and deformation of bubbles or volcanic welding of particles in dynamic heating or cooling scenarios.

Acknowledgments
The authors thank Taylor Witcher for valuable input and acknowledge funding provided by the European Research Council advanced grant EVOKES (247076), the UK's Natural Environment Research Council grant NE/N002954/1, and the AXA Research Fund Grant "Risk from Volcanic Ash in the Earth Environment." We acknowledge editorial handling by Michael Walter, and comments on a previous version of this manuscript by Andrew V. Newman and anonymous reviewers all of whom greatly improved the clarity of the work. Simulation data pertaining to this work are available from the authors upon request via fabian.wadsworth@min.uni-muenchen.de.

References

Aizawa, K., C. Cimarelli, M. Alatorre-Ibargüengoitia, A. Yokoo, D. Dingwell, and M. Iguchi (2016), Physical properties of volcanic lightning: Constraints from magnetotelluric and video observations at Sakurajima volcano, Japan, *Earth Planet. Sci. Lett.*, *444*, 45–55.

Angell, C. A., K. L. Ngai, G. B. McKenna, P. F. McMillan, and S. W. Martin (2000), Relaxation in glassforming liquids and amorphous solids, *J. Appl. Phys.*, *88*(6), 3113–3157, doi:10.1063/1.1286035.

Bagdassarov, N., and D. Dingwell (1994), Thermal properties of vesicular rhyolite, *J. Volcanol. Geotherm. Res.*, *60*(2), 179–191.

Behnke, S., and S. McNutt (2014), Using lightning observations as a volcanic eruption monitoring tool, *Bull. Volcanol.*, *76*(8), 847.

Berman, R. (1953), The thermal conductivity of dielectric solids at low temperatures, *Adv. Phys.*, *2.5*, 103–140.

Cimarelli, C., M. Alatorre-Ibargüengoitia, U. Kueppers, B. Scheu, and D. Dingwell (2014), Experimental generation of volcanic lightning, *Geology*, *42*, 79–82.

Cimarelli, C., M. Alatorre-Ibargüengoitia, K. Aizawa, A. Yokoo, A. Diaz-Marina, M. Iguchi, and D. Dingwell (2016), Multiparametric observation of volcanic lightning: Sakurajima Volcano, Japan, *Geophys. Res. Lett.*, *43*, 4221–4228, doi:10.1002/2015GL067445.

Crank, J. (1975), *The Mathematics of Diffusion*, Clarendon, Oxford.

Di Genova, D., C. Romano, D. Giordano, and M. Alletti (2014), Heat capacity, configurational heat capacity and fragility of hydrous magmas, *Geochim. Cosmochim. Acta*, *142*, 314–333.

Dingwell, D. B., and S. L. Webb (1989), Structural relaxation in silicate melts and non-Newtonian melt rheology in geologic processes, *Phys. Chem. Miner.*, *16*(5), 508–516.

Farzaneh, M., and W. Chisholm (2009), *Insulators for Icing and Polluted Environments*, 706 pp., John Wiley.

Gardner, J. E., and R. A. Ketcham (2011), Bubble nucleation in rhyolite and dacite melts: Temperature dependence of surface tension, *Contrib. Mineral. Petrol.*, *162*(5), 929–943.

Genareau, K., J. Wardman, T. Wilson, S. McNutt, and P. Izbekov (2015), Lightning-induced volcanic spherules, *Geology*, *43*(4), 319–322.

Giehl, C., R. Brooker, H. Marxer, and M. Nowak (2016), An experimental simulation of volcanic ash deposition in gas turbines and implications for jet engine safety, *Chem. Geol.*, in press.

Gottsmann, J., D. Giordano, and D. B. Dingwell (2002), Predicting shear viscosity during volcanic processes at the glass transition: A calorimetric calibration, *Earth Planet. Sci. Lett.*, *198*(3), 417–427.

Heiken, G. (1974), An atlas of volcanic ash, NASA Tech. Rep., NASA-TM-X-.

Hess, K. U., and D. B. Dingwell (1996), Viscosities of hydrous leucogranitic melts: A non-Arrhenian model, *Am. Mineral.*, *81*(9–10), 1297–1300.

Kueppers, U., C. Cimarelli, K.-U. Hess, J. Taddeucci, F. B. Wadsworth, and D. B. Dingwell (2014), The thermal stability of Eyjafjallajökull ash versus turbine ingestion test sands, *J. Appl. Volcanol.*, *3*(1), 4, doi:10.1186/2191-5040-3-4.

Lange, R. A., and I. S. E. Carmichael (1987), Densities of Na_2O-K_2O-MgO-MgO-FeO-Fe_2O_3-Al_3O_3-TiO_2-SiO_2 liquids: New measurements and derived partial molar properties, *Geochim. Cosmochim. Acta*, *51*, 2931–2946.

Lee, D. W., and W. D. Kingery (1960), Radiation energy transfer and thermal conductivity of ceramic oxides, *J. Am. Ceram. Soc.*, *43*, 594–607.

Liu, E., K. Cashman, and A. Rust (2015), Optimising shape analysis to quantify volcanic ash morphology, *Geophys. Res. J.*, *8*, 14–30.

Liu, Y., Y. Zhang, and H. Behrens (2005), Solubility of H_2O in rhyolitic melts at low pressures and a new empirical model for mixed H_{2O}–CO_2 solubility in rhyolitic melts, *J. Volcanol. Geotherm. Res.*, *143*(1), 219–235.

Llewellin, E. W., H. M. Mader, and S. D. R. Wilson (2002), The rheology of a bubbly liquid, *Proc. R. Soc. London, Ser. A*, *458*(2020), 987–1016.

McNutt, S., and E. Williams (2010), Volcanic lightning: Global observations and constraints on source mechanisms, *Bull. Volcanol.*, *72*(10), 1153–1167.
Paxton, A., R. Gardner, and L. Baker (1986), Lightning return stroke: A numerical calculation of the optical radiation, *Phys. Fluids*, *29*, 2736–2741.
Pijpers, T. F., V. B. Mathot, B. Goderis, R. L. Scherrenberg, and E. W. van der Vegte (2002), High-speed calorimetry for the study of the kinetics of (de) vitrification, crystallization, and melting of macromolecules, *Macromolecules*, *35*(9), 3601–3613.
Rakov, V. (2013), The physics of lightning, *Surv. Geophys.*, *34*(6), 701–729.
Rallison, J. (1984), The deformation of small viscous drops and bubbles in shear flows, *Annu. Rev. Fluid Mech.*, *16*(1), 45–66.
Russell, J. K., D. Giordano, and D. B. Dingwell (2003), High-temperature limits on viscosity of non-Arrhenian silicate melts, *Am. Mineral.*, *88*(8–9), 1390–1394, doi:10.2138/am-2003-8-924.
Schiaffino, S., and A. A. Sonin (1997), Molten droplet deposition and solidification at low Weber numbers, *Phys. Fluids*, *9*(11), 3172–3187.
Shinozaki, M., K. A. Roberts, B. van de Goor, and T. W. Clyne (2013), Deposition of ingested volcanic ash on surfaces in the turbine of a small jet engine, *Adv. Eng. Mater.*, *15*(10), 986–994.
Song, W., K. Hess, D. E. Damby, F. B. Wadsworth, Y. Lavallée, C. Cimarelli, and D. B. Dingwell (2014), Fusion characteristics of volcanic ash relevant to aviation hazards, *Geophys. Res. Lett.*, *41*, 2326–2333, doi:10.1002/2013GL059182.
Song, W., Y. Lavallée, K. U. Hess, U. Kueppers, C. Cimarelli, and D. B. Dingwell (2016), Volcanic ash melting under conditions relevant to ash turbine interactions, *Nat. Commun.*, *7*, doi:10.1038/ncomms10795.
Stroberg, T. W., M. Manga, and J. Dufek (2010), Heat transfer coefficients of natural volcanic clasts, *J. Volcanol. Geotherm. Res.*, *194*(4), 214–219.
Taylor, G. (1934), The formation of emulsions in definable fields of flow, *Proc. R. Soc. London, Ser. A*, *146*, 501–523.
Wadsworth, F. B., J. Vasseur, F. W. Aulock, K. Hess, B. Scheu, Y. Lavallée, and D. B. Dingwell (2014), Nonisothermal viscous sintering of volcanic ash, *J. Geophys. Res. Solid Earth*, *119*, 8792–8804, doi:10.1002/2014JB011453.
Wadsworth, F. B., J. Vasseur, E. W. Llewellin, J. Schauroth, K. J. Dobson, B. Scheu, and D. B. Dingwell (2016), Sintering of viscous droplets under surface tension, *Proc. R. Soc. London, Ser. A*, *472*(2188), 20150780.
Wardman, J., T. Wilson, P. Bodger, J. Cole, and D. Johnston (2012), Investigating the electrical conductivity of volcanic ash and its effect on HV power systems, *Phys. Chem. Earth, Parts A/B/C*, *45–46*, 128–145.